Experimental study of dispersed oil-water flow in a horizontal pipe with enhanced inlet mixing,
Part 2: In-situ droplet measurements

Heiner Schümann[1,2]*, Murat Tutkun[3,4], Ole Jørgen Nydal[1]

[1]Department of Energy and Process Engineering, Technical University of Science and Technology, NTNU, Trondheim, Norway
[2]Multiphase Flow Laboratory, SINTEF Petroleum AS, Trondheim, Norway
[3]Department of Fluid Flow Technology, Institute for Energy Technology, Kjeller, Norway
[4]Department of Mathematics, University of Oslo, Oslo, Norway

*Corresponding author, Email: heiner.schumann@ntnu.no

Abstract

Droplet size measurements in premixed oil-water flow are presented. Three traversable focused beam reflectance measurement probes (FBRM) positioned along the test section allowed for measuring averaged droplet size profiles over the cross section. Measurements for two mixture velocities, U_{mix} = 0.5 m/s and U_{mix} = 1 m/s, and the complete range of input water fractions were performed with tap water and medium viscosity mineral oil. The flow facility provided a *10 cm* inner diameter test section of *24 m* total length. Flow development in terms of droplet growth was documented. Averaged droplet sizes showed to be a function of the dispersed phase fraction with sizes increasing towards a maximum at phase inversion. Different flow patterns show characteristic droplet size profiles over the cross-section. Common models over-predict the presented droplet size data, most probably as a result of enhanced inlet mixing and underdeveloped flow.

1. Introduction

Pipe flow of liquid-liquid dispersions is common in the process industry. Transport of oil-water dispersions in oil production systems is difficult to predict and often requires special attention. Formation of emulsion affects not only individual components like separators, pumps or pipelines, but also overall flow assurance (Lim et al., 2015). One of the key issues in oil-water dispersed flow is size and dynamics of droplets. Detailed in-situ measurements of droplets, therefore, are necessary to gain more insight into dispersed flows. This, in turn, will help us to improve simulation tools as well as our predicting capacity and flow control strategies. These eventually lead to cost reduction and increased safety.

It is a known fact that any change in droplet size distribution within the flow is always accompanied by change in rheology of emulsion (Pal, 1996). A reduction in droplet size was found to increase the effective viscosity. In some cases the presence of droplets can lead to drag reduction as result of turbulence modification in the flow (Angeli and Hewitt, 1999; Pal, 1993). In a similar manner, droplet size reacts on changes in the flow. Higher mixture velocities for instance will reduce droplet sizes as a consequence of enhanced break-up. At higher dispersed phase fractions coalescence becomes more active and droplet sizes increase (Ioannou, 2006; Ward and Knudsen, 1967). Droplets can further be influenced by adding stabilizing agents, the so-called surfactants, to the flow.

Droplets arise from instabilities at the liquid-liquid interface at sufficiently high flow rates. In more realistic oil-water transport systems, however, a dispersion usually forms in the reservoir (Cabellos et al., 2009). Flow control units like mixers, pumps and valves add additional droplets as the flow passes through them (Middleman, 1974; Morales et al., 2013; Noïk et al., 2005; van der Zande and van den Broek, 1998). Eventually this develops towards a final droplet size distribution which is controlled by simultaneous break-up and coalescence in the system.

Droplet size distributions in horizontal oil-water dispersed flow with a low viscosity oil ($1.6\ mPa*s$) were measured by Angeli and Hewitt (2000) using an endoscope camera. A T-junction and low dispersed phase inlet velocities ensured break-up in the test section and not at the inlet. At equal mixture velocities and dispersed phase fractions, droplets were found to be smaller in oil continuous flow compared to water continuous flow. In the tested range ($3.4-9\%$) the dispersed phase fraction did not seem to influence the droplet size.

Simmons and Azzopardi (2001) found droplet size stratification at low velocities in a horizontal pipe section, using kerosene as continuous phase and potassium carbonate solution as dispersed phase. Hinze (1955) theory agreed well with droplet size measurements for low dispersed phase

fractions only. A special inlet device in this case prevented dispersion formation due to the merging of the phases.

El-Hamouz and Stewart (6-9 October 1996) used a Par-Tec M300 laser backscatter instrument to investigate droplet sizes in oil-water flow through different pipe fittings and geometries. Even if the oil-water volumetric ratio was low (i.e., 1:50) droplet growth downstream of the inlet was measured.

Middleman (1974) measured water continuous dispersions formed in pipe flow through a static mixer. A positive effect of dispersed phase fraction and viscosity on the mean droplet size was found.

Droplets in dual-continuous flow were measured by Lovick and Angeli (2004) with help of a dual sensor impedance probe. This study mainly concerned the chord lengths instead of actual droplet size and showed that chord size was largest at the interphase. Furthermore, high shear in the pipe wall region was found to reduce droplet sizes.

In a study by Ioannou (2006) droplet sizes of oil and water continuous flow at high mixture velocities ($U_{mix} = 3.0$, 3.5 and $4.0\ m/s$) before and after phase inversion are presented. Cross sectional averaged means peaked at phase inversion point.

This paper focuses on the development of unstable dispersions downstream of a static mixer. We present new experimental data which are also compared to existing droplet size models. We utilized a focused beam reflectance measurement (FBRM) system and further investigate the applicability of the FBRM as a tool for in-situ droplet measurements in liquid-liquid pipe flow. Of particular interest is the possibility to distinguish certain flow regimes based on droplet size measurements.

2. Experimental setup

Experimental facility is the Well Flow Loop of the Institute for Energy Technology (IFE) in Kjeller, Norway. The transparent PVC test section has a total length (L) of 25 m and inner diameter (D) of 100 mm. Oil and water were mixed at the inlet of the test section. Enhanced mixing was ensured by a static mixer installed right after the section where oil and water were injected into the pipe. The flow therefore was initiated in a premixed state.

The test section was horizontally aligned (0°±0.1°). Figure 1 shows a schematic of the test section. The pressure gradient was measured over three separate sections along the pipe. A broad beam gamma densitometer and an X-ray tomography instrument provided local phase fraction measurements. Video recordings and visual observations were used to identify flow patterns. Three traversable FBRM probes collected data at three different downstream locations for in-situ droplet characterization. A more detailed experimental description as well as flow pattern, pressure drop and phase fraction measurements were presented in (Schümann et al.).

Droplets were measured at two different mixing velocities: $U_{mix} = 0.5\ m/s$ and $1\ m/s$. These measurement were carried out for input water fractions changing from 0% to 100 % with 10% intervals.

2.1 Fluid properties

Tap water and mineral oil mixtures were the test fluids. The experiments were repeated for three different oil viscosities as summarized in Table 1. The flow loop was temperature controlled and a liquid temperature of 20± 0.5°C was kept for all experiments. Input water fractions needed for phase inversion were typically in the range of $20\% < f_{w\_inv} < 30\%$ for these oil mixtures. f_{w_inv} was smallest for oil A and largest for oil C.

Table 1: Properties of the tested mineral oil mixtures.

Oil	Composition Primol 352: Exxsol D80	Density [kg/m^3]*	Viscosity [mPa*s]*	Interf. tension [mN/m]** (short/long term)
Oil A	25:1	866 (±0.2%)	120 (±3%)	23/14 (±10%)
Oil B	6:1	859 (±0.2%)	60 (±2%)	23/14 (±10%)
Oil C	4:1	853 (±0.2%)	35 (±2%)	24/15 (±10%)
Tap water	-	999	1	-

*Viscosity was measured at 20 C. Viscosity uncertainties due to temperature fluctuations are considered in the uncertainties.
** With tap water

2.2 FBRM (Focused beam reflectance measurement)

The FBRM is a widely used in-situ particle characterization tool. A focused laser beam with negligible width rotates at high speed and scans the flow. Whenever the laser crosses a particle or a droplet, backscattered light is measured by a sensor. An algorithm distinguishes between different chord lengths corresponding to the scanned particles. In this way the FBRM automatically counts thousands of droplets within a short period of time. After a predefined sampling interval (15 sec in our case) a chord length distribution is computed and stored. 15 sec was found to be long enough to give sufficient numbers of counts to produce smooth size distributions. At the same time it was short enough to identify eventual fluctuations and changes of the flow. The scanned circle has a diameter of $8\ mm$. The size limit, however, is smaller. The software allows measuring chord lengths up to $4\ mm$. For chord lengths larger then $1\ mm$ one can expect the influence of the curvature of the circle to become important. More technical details regarding the instrument and principles of operation are documented in Schümann et al. (2015).

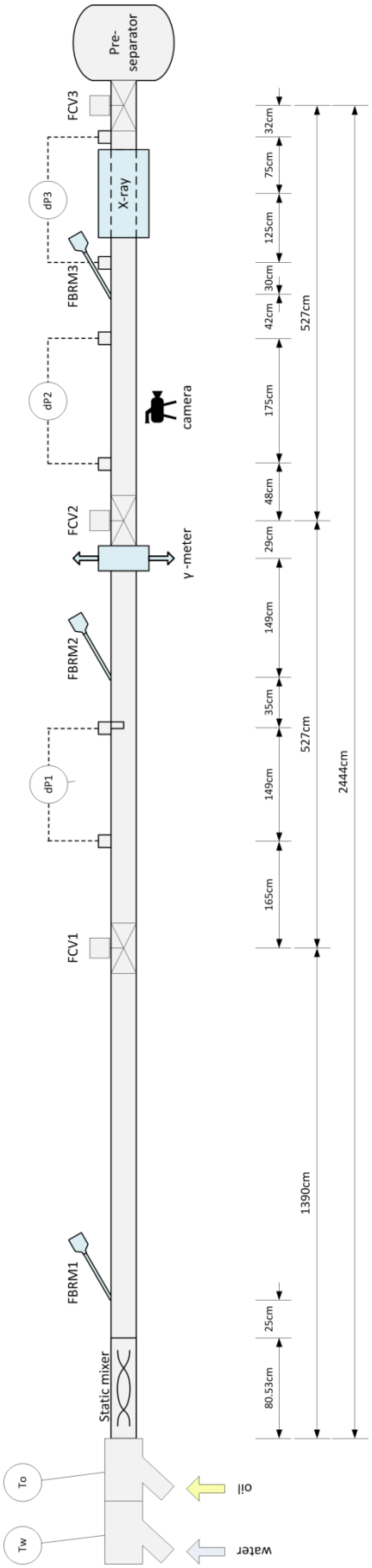

Figure 1: Test section.

Three FBRM probes (by Mettler Toledo) of type D600 were mounted in adapters as shown in Figure 2. The probes were aligned 45° against the flow. The adapters were specially designed to allow traversing into the pipe to measure different position in vertical direction. Five measurements were chosen as measurement locations and they were distributed symmetrically around the center point; e.g. +/- 4 cm, +/- 2cm and 0. In this way we were also able to obtain a coarse vertical droplet size profile over the cross section of the pipe.

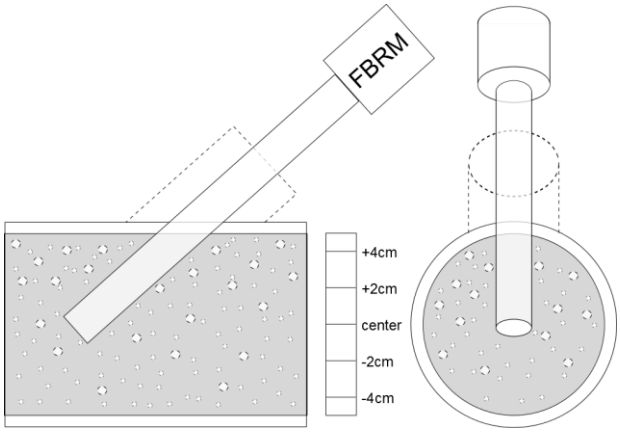

Figure 2: Sketch of the traversable FBRM mounted in an adapter. The flow direction was from left to right for the figure showing the side view.

Every measurement probe inserted into the pipe is intrusive. A strict procedure was followed in order to minimize flow disturbances by the probe. Local phase fractions and pressure gradients were measured with the probes extracted to its maximum at the beginning of an experiment. Afterwards, the probes were traversed through the cross section starting with the probe at the end of the test section. When all measurements at the five vertical sample positions were obtained, this procedure was repeated by with middle probe and finally the last probe. In this way, upstream probes did not disturb the downstream measurements. Another issue is the influence of the flow field just in front of the probe. Unfortunately, this issue cannot be avoided. Streamlines of the flow will go around the probe. While the smallest droplets might follow the streamlines, the largest droplets will impact due to larger inertia. Such an effect would be dependent on the flow velocity and water fraction. In this case the droplet size distributions measured by the FBRM would be most affected at the lower end of the spectrum, representing the smallest droplets, because these droplets have a higher chance of escaping from the measurement volume. We would therefore expect to see such an influence in the lower spectrum comparing measurements for the same experiment from the highest and lowest measurement points, close to the wall where the flow velocity is lowest, with the center of the pipe. A distinct difference was, however, not found from the measurements. Also, the Sauter mean diameter, D_{32}, mainly presented in this paper, is little sensitive to the smallest droplets.

2.3 Data processing

The chord length distribution measured by the FBRM differs from the real droplet size distribution due to several reasons: (i) The laser beam does not necessarily cross a droplet in the center every time the laser hits the droplet, which would automatically lead to the correct diameter. The laser beam crossing the droplet through off-center points introduces an underestimation of the droplet size. (ii) In dense emulsions scattering of light by other droplets can lead to a misinterpretation of the measured signal. (iii) Differences in the refractive index of the liquids as well as rough droplet surfaces on the micro scale can further influence the backscattering.

In order to reduce the underestimation of droplet size, we developed a methodology of calibrating the FBRM using an optical in-situ measurement technique (Particle Video Microscopy – PVM) (Schümann et al., 2015). This methodology was able to provide real droplet sizes with an uncertainty of 50%. This conversion was applied to the measurements presented in this study. Therefore, we will present our results in terms of droplet size, meaning the diameters of individual droplets, instead of chord lengths, which is what one can get from the FBRM.

A main problem of the FBRM, called probe coating, occurs if single droplets stick to the probe window. In this case a continuous sampling of the same droplets creates large peaks in the chord length distribution. Furthermore, such peaks affect mean sizes derived from the distribution curves. We noticed that probe coating in this study occurred for single samples only and stuck droplets were washed away again automatically. The software which we used in our measurement monitors the samples real time and it was easy to catch probe coating problem immediately. Throughout the experimental campaign several samples were taken for every data point. In a manual screening, later, samples where probe coating occurred were rejected. The accepted samples were then averaged in order to reach final and actual chord length distributions.

3. Results

3.1 *Cross sectional droplet size distribution*

In this section we investigate cross sectional characteristics of the droplet size and try to identify specific flow regimes. Considering the measurement uncertainty results were similar for the different oils. Here we will focus on oil C. With the lowest viscosity of the three tested oils, probe coating was least problematic and results most clear. Also, unless otherwise specified the presented results are based on measurements by FBRM probe 3, where the flow is most developed.

In order to better understand the following results we will recall the cross sectional water line-measurements, Figure 3 and Figure 4, as presented in Schümann et al. (). At $U_{mix} = 0.5\ m/s$ the flow was semi-dispersed. For input water fractions less than 50%, the flow was three-layered with a layer of pure oil on top, a dispersed layer in the middle, and a pure water layer at the bottom. A pure water layer was not present for the lowest input water fraction. Higher input water fractions resulted in a water continuous flow with a dense packed layer of oil droplets in the upper part of the pipe. Here, the pure oil layer disappeared. At $U_{mix} = 1\ m/s$ the flow was fully dispersed, either water continuous or oil continuous. We observed a dual continuous flow pattern only for oil C around the inversion point, $f_w = 0.31$.

Cross sectional water fraction measurements are presented together with Sauter mean diameters, D_{32} at the particular measurement positions in Figure 5 and Figure 6. The presented water fraction measurements and tomographic reconstructions were obtained from X-ray measurements described in detail in Schümann et al. (). The Sauter mean diameter is calculated as

$$D_{32} = \sum_{i=1}^{k} n_i D_i^{\,3} \Big/ \sum_{i=1}^{k} n_i D_i^{\,2} \qquad (1)$$

where D_i is the median of a particular bin i with the number of counts n_i. For a volumetric dispersed phase fraction Φ the D_{32} allows for directly obtaining the interfacial area per unit volume (Middleman, 1974):

$$A_v = 6\Phi / D_{32} \qquad (2)$$

Figure 5 shows the three typical cases for $U_{mix} = 0.5\ m/s$ with different positions of the dispersion layer.

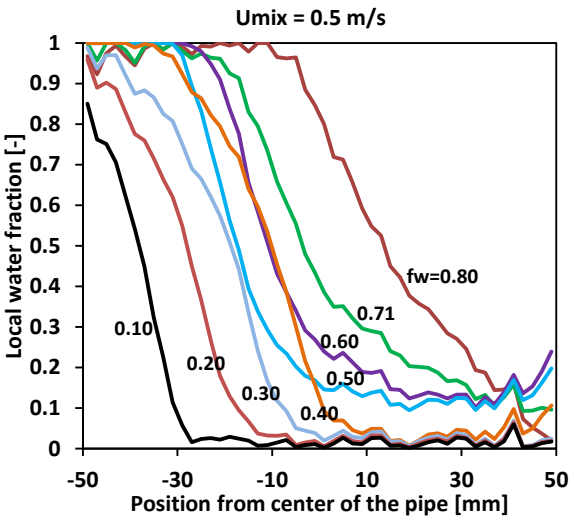

Figure 3: Water line fraction measurements for Oil C (*35 mPa*s*) at $U_{mix} = 0.5 m/s$. The input water fractions, f_w, are shown in the figure. Results from Schümann et al. ().

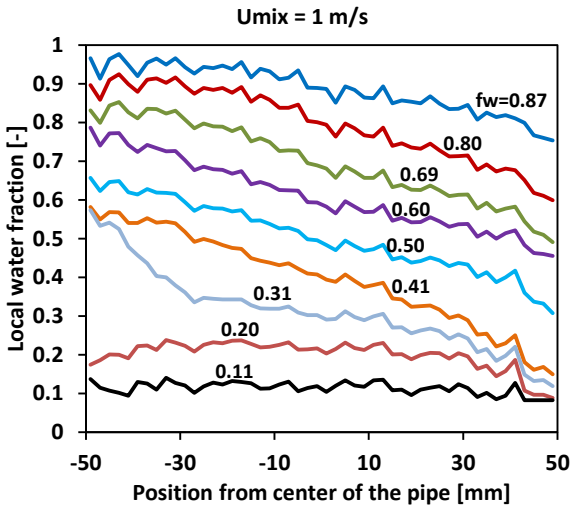

Figure 4: Water line fraction measurements for Oil C (*35 mPa*s*) at U_{mix} = *1m/s*. The input water fractions, f_w, are shown in the figure. Results from Schümann et al. ().

Comparison of the D_{32} values in the upper and lower part of the dispersed layer indicates some distinct features of a three-layered flow pattern. This means that the dispersed layer was divided into a region of dispersed water droplets in oil, which formed the upper part, and a region of oil droplets in water, which formed the lower part. In the upper layer, water droplets (D_{32}) typically were less than $0.5\,mm$. Oil droplets in the lower layer were in the range of *1 mm* to *2.5 mm*. When f_w *> 50%,* droplet sizes were more uniform. This essentially confirms the assumption that the dispersion is of oil-in-water type for these input water fractions.

Figure 6 shows measurements for oil continuous flow ($f_w = 20\%$), dual continuous flow ($f_w = 31\%$), and water continuous flow ($f_w = 80\%$).

For oil continuous flow (f_w *= 20%)* the dispersed phase was homogeneously distributed over the cross section. A slightly lower concentration of dispersed phase close to the pipe wall can be attributed to the near wall effect which essentially leads to a reduced mixing due to the substantial drop of velocity. Droplet size measurements demonstrate that the largest droplets are mainly in the center of the pipe with a decreasing size towards the wall. Even if detailed local velocity and turbulence measurements are missing, one can assume the following: Considering the presence of a inlet mixer and a Reynolds number of *Re = 2400* based on oil properties, the flow might be turbulent. The shear around the pipe centerline is very low compared to the shear one observes near the wall. The level of turbulence also drops significantly around the centerline. Due to these effects, the level of break-up process around the centerline is not very high, which eventually results in larger droplets. High shear near the wall together with large turbulent fluctuations enhance the break-up process and droplet size drops accordingly.

For water continuous flow (f_w *= 80%*) the dispersed oil fraction and droplet size increase simultaneously with the height. As the oil blends into the water, then the local viscosity increases. This leads to lower turbulence intensity, hence larger droplets. In addition, larger droplets will settle faster towards the top of the pipe and increasing dispersed phase fraction promotes coalescence.

The dual-continuous case is presented by f_w *= 31%*. Even though the boundary between oil continuous and water continuous regions is difficult to identify, we expect it to be around -25 mm from the centerline where we observe the slope change in water fraction profile.

Sauter mean diameters over the cross section for all measured input water fractions at $U_{mix} = 1\ m/s$ are shown in Figure 7. Droplet sizes increase as the dispersed phase fraction does, which is the case for both water and oil-continuous flow. A stratification of the droplet size, with increasing mean sizes towards the pipe top, is observed for high input water fractions, f_w *= 0.87, 0.8 and 0.69*. A similar stratification for oil continuous flow is also documented in Simmons and Azzopardi (2001). For lower input water fractions, fw = 0.6, 0.5 and 0.41, a size reduction also towards the upper pipe wall was measured. Thus, the largest droplets were measured in the center of the pipe. Again, high shear close to the wall enhances the break-up process and leads to a decreasing droplet size profile toward the wall. This has also been observed by Lovick and Angeli (2004) as droplet measurements close to the interface in dual continuous flow showed a profile of smaller droplets toward the wall. . The interface close to the pipe wall did have no large droplets.

We found following relation between mean and maximum droplet size:

$$D_{32} = cD_{\max} \tag{3}$$

This is in agreement with our previous findings as documented in Schümann et al. (2015). This relation was first mentioned in Sprow (1967) regardless of the shape of a DSD and of the mixing intensity. A value of $c = 0.61$ with a standard deviation (std(c)) of 0.03 was obtained from the converted DSD. Similar c values have already been documented by others: for gas bubbles 0.62 by Hesketh et al. (1987), 0.48 by Angeli and Hewitt (2000). The latter was due to the method of calculation since Angeli and Hewitt (2000) used the 95th percentile per volume, D_{95_vol}, as a measure for D_{max}. It was also reported by the authors that only 0.3% of the numbers of drops were larger than the D_{max}. In our work, however, the 99th percentile per number, D_{99_num}, was used. This naturally results in a larger value for c. Note that range of c values reported in literature in mixer experiments is from 0.38 to 0.7 (Brown and Pitt, 1972; Calabrese et al., 1986; Coulaloglou and Tavlarides, 1976; Giapos et al., 2005; Sprow, 1967; Zhou and Kresta, 1998).

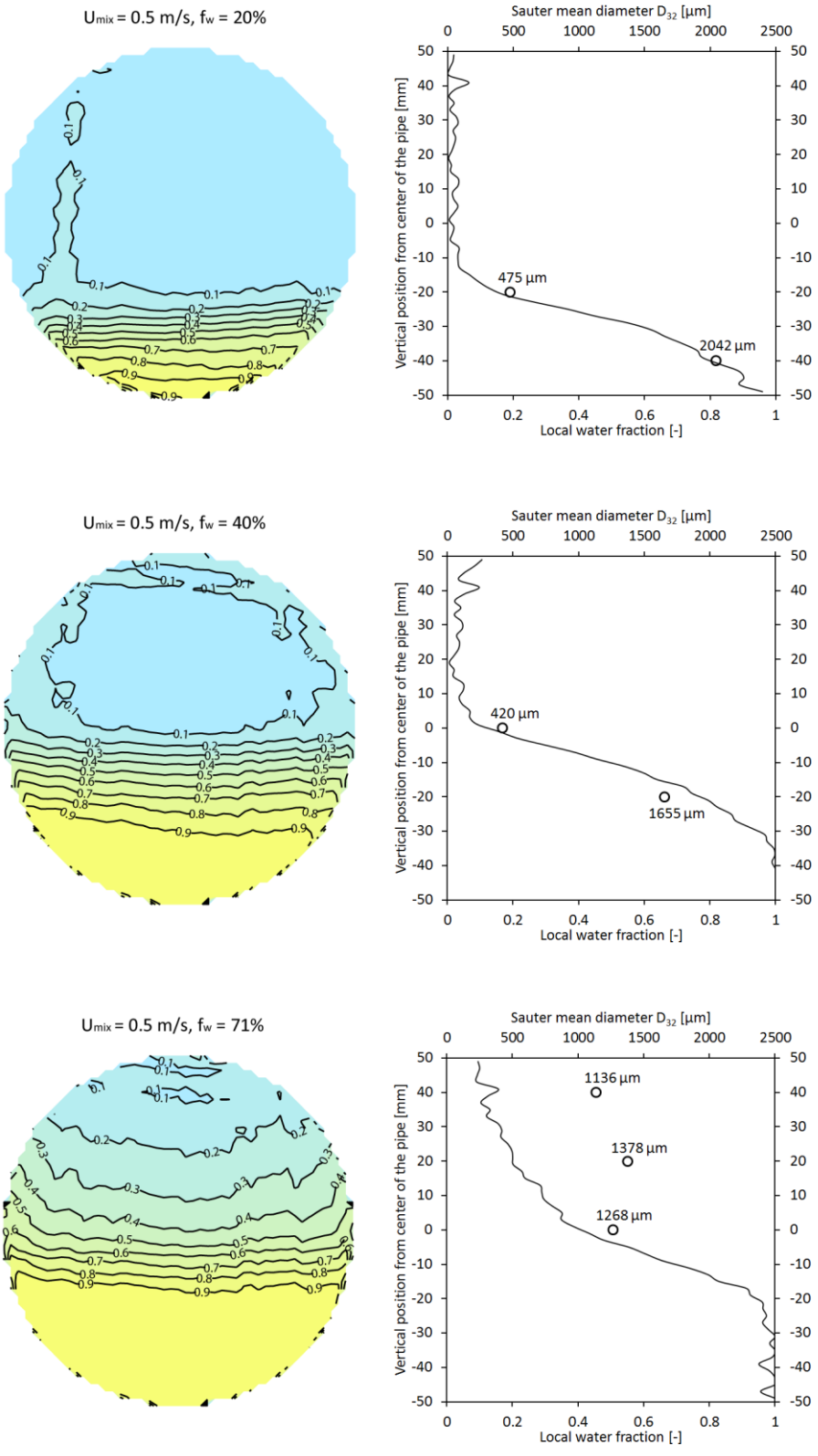

Figure 5: Selected measurements for U_{mix} = 0.5 m/s. Left column: Cross sectional water distribution. Contour lines show the local water fraction with an increment of 0.1. Right column: Water line fraction measurements and droplet sizes across the pipe. The uncertainty of the droplet sizes is approximately 50%.

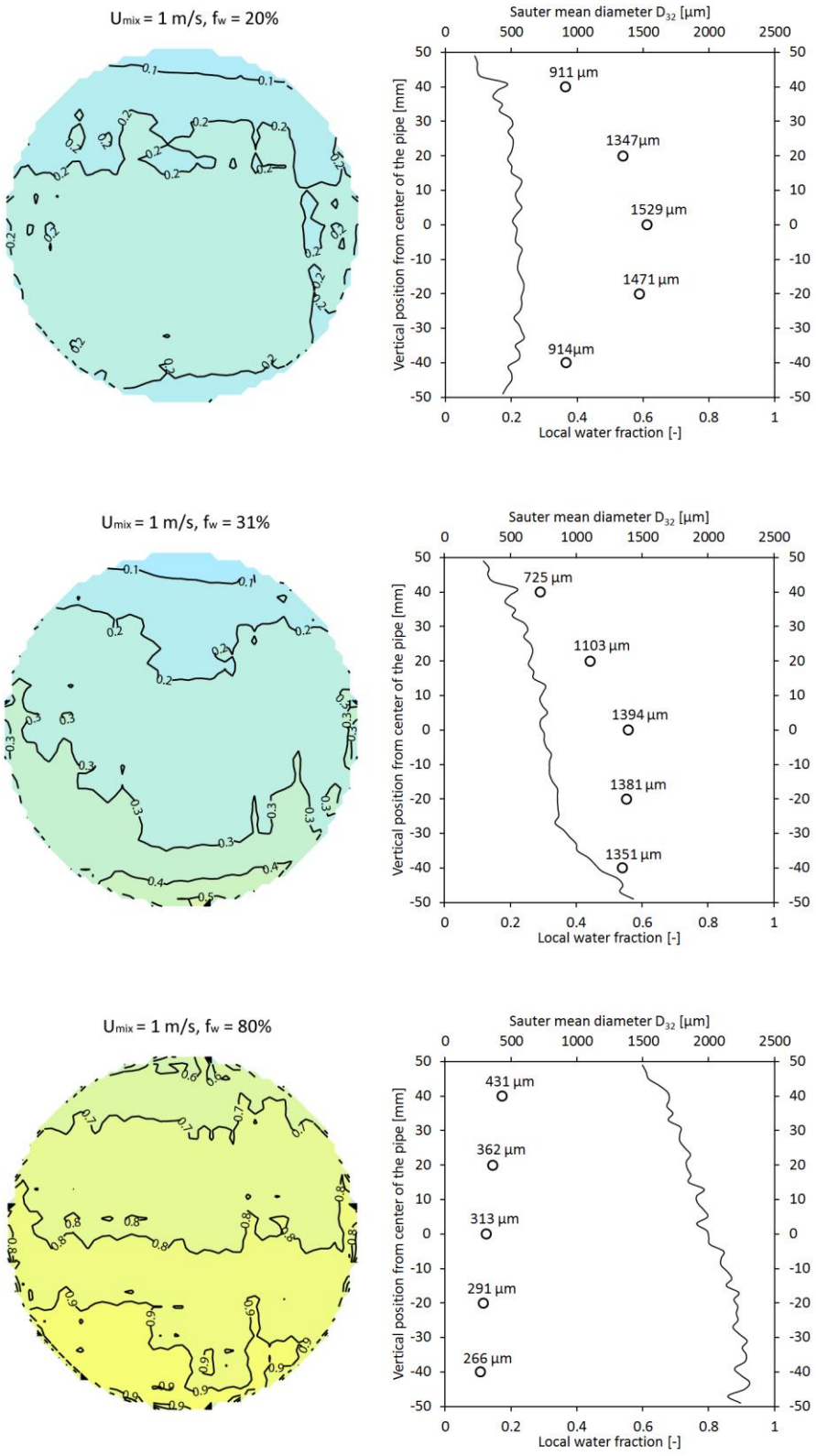

Figure 6: Selected measurements for U_{mix} = 1 m/s. Left column: Cross sectional water distribution. Contour lines show the local water fraction with an increment of 0.1. Right column: Water line fraction measurements and droplet sizes vs. the position in the pipe. The uncertainty of the droplet sizes is approximately 50%.

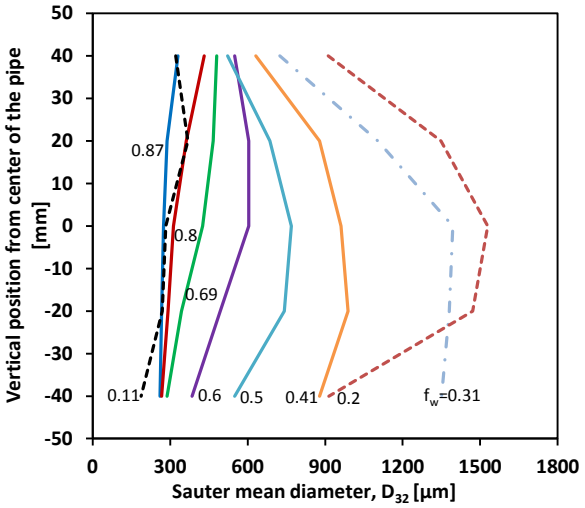

Figure 7: Droplet size profiles at different water-cuts at U_{mix}=1m/s. Data are taken by the FBRM 3 which was in the end of the test section. Continuous lines show water continuous flow, broken lines show oil continuous flow, dotted-broken line shows dual continuous flow. Note that the inversion point is at f_w of approximately 30%.

3.2 Influence of the phase fractions

Figure 7 shows the droplet size change across the pipe at different input water fractions. At each input water fraction we computed the average droplet size over the cross section. To do so, the chord length distributions obtained at each probe position were weighted according to the representative area of the cross section and the respective average dispersed phase fraction in this area. This is illustrated in Figure 8. The dispersed phase fraction was found from the vertical line fraction measurements. Consequently the weighted chord length distributions were averaged and converted to droplet sizes to obtain D_{32}. (Note that phase fraction differences in the horizontal direction were assumed to be negligible in this approach.)

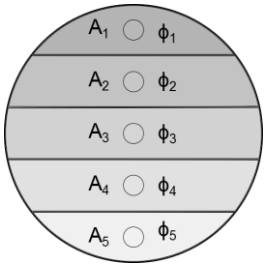

Figure 8: Cross sectional averaging A_i and ϕ_i. denote cross-sectional area of the probed segment, and the phase fraction in that area, respectively. i =1,…N, where N is the maximum number of mesurement positions where the FBRM is operated to collect data.

The result for the most downstream (and hence, most developed) measurement position at $U_{mix} = 1\ m/s$ is shown in Figure 9 for both oil A, B and C. The smallest droplets were found for the lowest dispersed phase fractions. The Sauter mean diameter, D_{32}, increases exponentially towards a peak value at phase inversion. The trend is similar to that of the pressure gradient as a function of input water fraction. Measurements performed using oil C reveal that the droplet size in a oil continuous flow increases dramatically shortly before the inversion. This distinct increase in the Sauter mean diameter right before phase inversion was also observed by others, cf. (Ioannou, 2006).

The oil viscosity herein plays a minor role. Droplets, however, seems to be slightly larger in the water continuous side. An increase in the droplet diameter with increasing dispersed phase viscosity was also observed by Ward and Knudsen (1967), and Middleman (1974) who state that "a high viscosity in the dispersed phase retards disruption of the drop". This is attributed to higher viscosity which leads to a higher energy dissipation during droplet deformation leaving less energy for the break-up process (van der Zande and van den Broek, 1998).

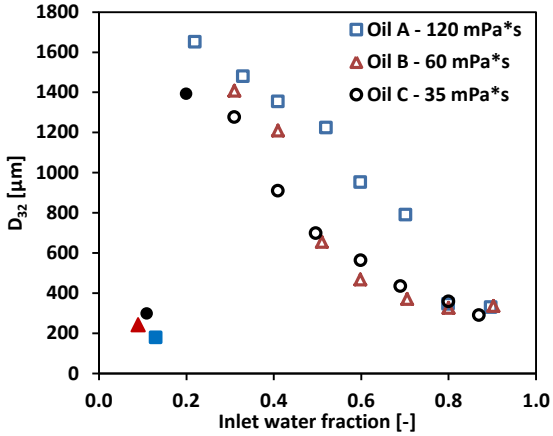

Figure 9: Sauter mean diameter, D_{32}, averaged over the cross section vs. inlet water fraction. U_{mix}=1m/s. Filled symbols show oil continuous flow, open symbols show water continuous flow.

The D_{32} close to the phase inversion point were of similar size for oil and water continuous flow, but as mentioned earlier the droplet size decreases faster with a decreasing dispersed phase fraction on the oil continuous side. Figure 10 shows the Sauter mean diameter as function of the real local dispersed phase fraction normalized by the dispersed phase fraction at the phase inversion. Best fitting curve using the least-squares method take the following form:

$$D_{32} = 2.5 \cdot 10^{-4} + 1.3 \cdot 10^{-3} \left(\phi / \phi_{inv} \right)^{2.7} \qquad (4)$$

Beside measurement uncertainties, the large spread of the data is due to the fact that a gradient of flow velocity inside the pipe creates different shear intensities across the cross section. In addition, the turbulence intensity profile in relation to the DSD variations is of importance (Simmons and Azzopardi, 2001).

Figure 10 further shows that the influence of the phase fraction is rather small when $\Phi/\Phi_{inv} < 0.2$. Also Angeli and Hewitt (2000) report no influence of the dispersed phase

fraction for dilute dispersions, e.g., the coalescence is insignificant for such cases. In their measurements the dispersed phase fraction was as high as 9%.

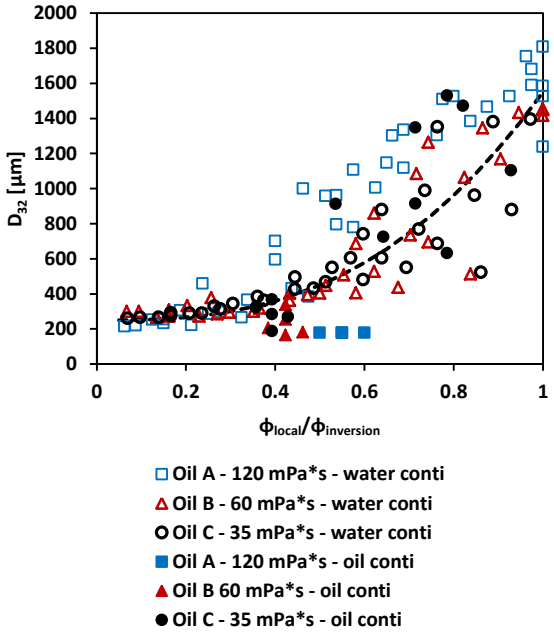

Figure 10: Local droplet size as a function of the local dispersed phase fraction for U_{mix}=1 m/s.

The rapid change of the DSD at phase inversion was measured in a separate experiment. Starting with oil continuous flow at $f_w = 10\%$, the input water fraction was slowly increased until the phase inversion was reached. Following the phase inversion, the water continuous flow regime stabilized at approximately $f_w = 30\%$. Then, the input water fraction was reduced again until the flow inverted back to oil continuity. Figure 11 shows the converted DSDs of the alternating oil/water continuous flow. Corresponding Sauter mean diameters are shown in Figure 12. The DSD and thus the D_{32} change considerably as the volumetric fraction of the dispersed phase are due to a change of the phase continuity at inversion.

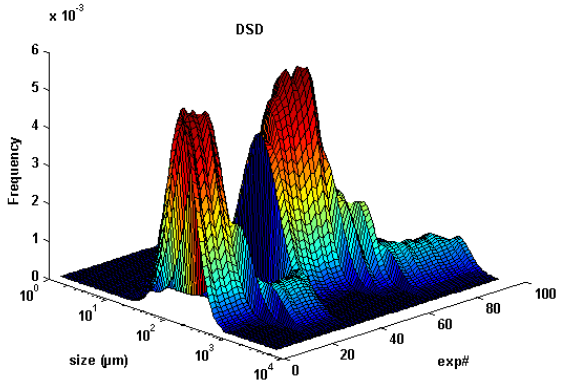

Figure 11: DSDs at phase inversion. The sampling time was 10 sec for each distribution.

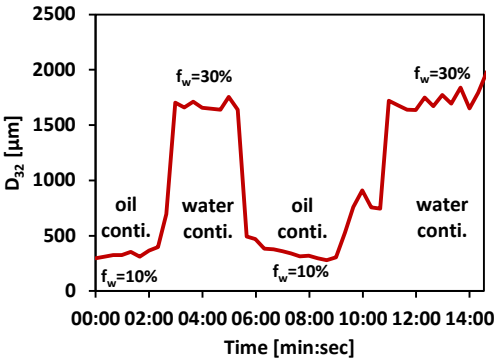

Figure 12: Sauter mean diameter in time through phase inversions.

3.3 Droplet growth

Flow development was obtained by pressure difference measurements along the pipe (Schümann et al.). This could be contributed to an in-flow separation behavior downstream of the static mixer. The flow was assumed to be well mixed when it leaves the static mixer at the pipe inlet. Settling of droplets is expected due to the buoyancy. This will produce the vertical gradient in the local dispersed phase fraction. When the flow is water continuous, larger oil droplets experience a stronger buoyancy force which leads to accumulation of these large droplets in the upper part of the pipe. Our cross sectional measurements as presented in section 3.1 indicate this as well. When the flow is, however, oil continuous the high viscosity of the oil presumably restricts a vertical drift of the water droplets.

The second mechanism is coalescence and break up of droplets as a result of the dynamics of the flow. If coalescence is dominating the droplet size will increase, while break up will lead to smaller droplet sizes. These affect the viscosity of the emulsion tremendously and can also impact to the state of flow (Pal, 1993; Pal, 1996).

These two mentioned mechanisms will influence each other as well. A higher dispersed phase fraction as a result of stratification will lead to higher coalescence rates. Larger droplets as a result of coalescence will lead to a faster stratification. Only at sufficiently high flow rates the mixing of the flow will overcome this separation behavior and break up can dominate.

In Figure 13 and Figure 14 the difference in the averaged Sauter mean diameter was compared between FBRM 1 and 2 and FBRM 2 and 3 respectively for $U_{mix} = 1m/s$. The change was expressed as a percentage growth rate per meter pipe section. Between FBRM 1 and 2 the growth rates are always positive. Oil C seems to grow slowest. However, the growth rates are very similar for oil A, B and C. At $f_w = 20\%$ oil C shows a peak, which might be due to partly inversion of the flow. A similar droplet growth downstream of a static mixer was also observed by (El-Hamouz and Stewart, 6-9 October 1996).

Between FBRM 2 and 3 the trend is less obvious. While oil droplets continue to grow for oil A, negative growth rates were measured for oil C. Oil B shows both.

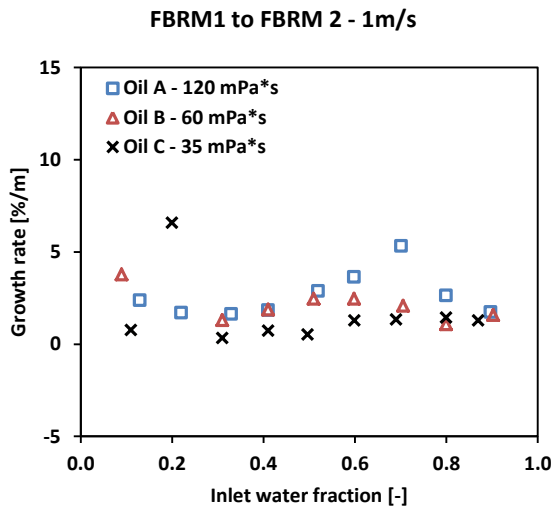

Figure 13: Relative droplet growth rate based on D_{32} between FBRM 1 and FBRM 2.

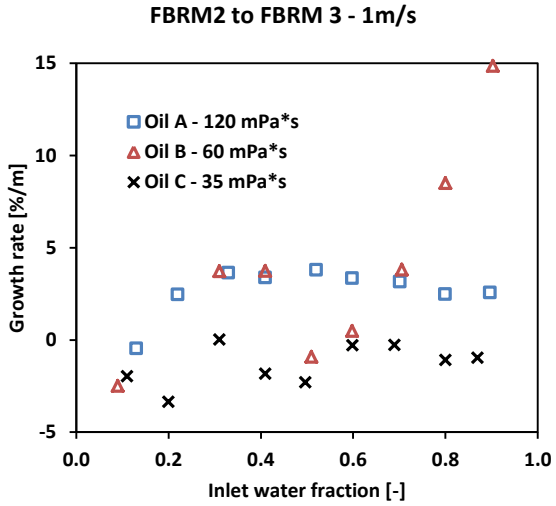

Figure 14: Relative droplet growth rate based on D32 between FBRM 2 and FBRM 3.

4. Comparison with droplet size models

The present data was compared with three models for the maximum droplet size. Results for oil C are shown in Figure 15. Models were tested for water continuous (long lines) and oil continuous (short lines) flow. The measured friction factors, f, were used in the models.

The classical model by (Hinze, 1955):

$$D_{\max}\left(\rho_c/\sigma\right)^{3/5}\varepsilon^{2/5}=0.725 \qquad (5)$$

with ε set equal to the mean energy dissipation rate per unit mass (Kubie and Gardner, 1977):

$$\varepsilon_M = 2fU^3/D \qquad (6)$$

overpredicted droplet sizes for the lowest dispersed phase fractions by a factor of four. An overprediction was expected as the DSD was initially produced by the inlet mixer. The large difference indicates that the flow cannot be characterized as fully developed yet. Considering the effect of the dispersed phase fraction, the Hinze model, originally developed for non-coalescing systems, is unable to predict the trend of increasing droplet sizes with higher dispersed phase fractions. Instead, the predicted D_{max} decreases due to an increasing friction factor, f.

Another model by Sleicher Jr. (1962) assumed droplet break-up taking place in the wall region mainly instead of isotropic turbulence as it was assumed by Hinze. Furthermore, both the viscosity of the continuous phase, μ_c, and dispersed phase, μ_d, were considered in the model:

$$\frac{D_{\max}\rho_c U_c}{\sigma}\sqrt{\frac{\mu_c U_c}{\sigma}}=38\left[1+0.7\left(\frac{\mu_c U_c}{\sigma}\right)^{0.7}\right] \qquad (7)$$

The Sleicher model better predicted D_{max} for the oil continuous case with the lowest dispersed phase fraction. For the water continuous experiments considerably larger droplets were predicted. Again the effect of the dispersed phase fraction could not be reproduced.

Only a model by Brauner (2001), as in equation (8), predicted the effect of the dispersed phase fraction for the water continuous flow well. This model was also the only one considering the dispersed phase fraction directly.

$$\frac{D_{\max}}{D}= 2.22C_H^{3/5}\left(\frac{\rho_c U_c^{\,2} D}{\sigma}\right)^{-0.6}\left[\frac{\rho_m}{\rho_c(1-\phi)}f\right]^{-0.4}\left(\frac{\phi}{1-\phi}\right)^{0.6} \qquad (8)$$

With the constant $C_H = 0.7$ the predicted D_{max} was in agreement with the Hinze model for the lowest dispersed phase fractions. By substituting the dispersed phase fraction, Φ, with the normalized dispersed phase fraction, Φ/Φ_{inv}, (shown as Brauner_rel in Figure 15) a steeper increase of the droplet size towards the phase inversion point was achieved.

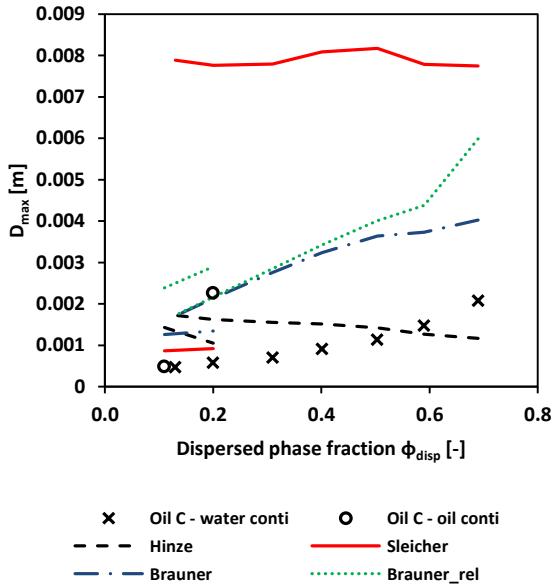

Figure 15: Comparison with droplet size models.

Comparing with the literature it was obvious that in experiments where the test section inlet prevented mixing and droplets arose as a result of the dynamics of the flow (Al-Wahaibi and Angeli, 2008; Angeli and Hewitt, 2000; Lovick and Angeli, 2004; Simmons and Azzopardi, 2001) droplets were larger than predicted by the Hinze, Sleicher or Brauner model. In this work droplets were smaller than predicted by these models.

5. Conclusion

Droplet size measurements in semi and fully dispersed horizontal oil-water pipe flow were presented. An FBRM instrument was used and the chord length data converted to droplet sizes using the calibration technique documented in Schümann et al. (2015). The FBRM instrument provided good stream of data in all tested situations. Cross sectional mean droplet size profiles, obtained from measurements at five different vertical positions, could be correlated with observed flow regimes. Its robustness, unrestricted range of use and the potential to indicate the flow pattern could make the FBRM to a useful tool not only for experimentation but also as control and optimization tool for oil production systems.

Dispersions were produced in a static mixer at the test section inlet. With FBRM measurements at three different positions along the pipe droplet growth downstream of the mixer could be shown. The Sauter mean diameter averaged over the cross section increased with the dispersed phase fraction. This dependency was also achieved when local measurements over the cross section were compared. Only a maximum droplet size model by Brauner (2001) was able to predict such a behavior.

Droplet size profiles over the cross-section show a stratification of droplet sizes, which was more distinct for water continuous flow. Also, for certain measurements of higher dispersed phase fractions smaller droplet sizes were measured close to the wall compared to the pipe center. This could indicate regions of high shear close to the wall leading to stronger break-up.

Droplet growth downstream of the mixer was shown comparing measurements of succeeding FBRM probes. Further downstream the pipe the behavior was less obvious. Also decreasing droplet sizes were observed. The viscosity of the oil seems to play a role as well. Further study is needed to better understand this phenomenon.

6. Acknowledgements

The authors acknowledge the financial support from The Multiphase Flow Assurance Innovation Centre (FACE). FACE is a research cooperation between IFE, NTNU and SINTEF. The centre is funded by The Research Council of Norway and by the following industrial partners: Statoil ASA, GE Oil & Gas, SPT Group - A Schlumberger Company, FMC Technologies, CD-adapco, Shell Technology Norway.

The authors further acknowledge Statoil ASA for the provision of the FBRM instruments used in this study.

7. References

Al-Wahaibi, T., Angeli, P., 2008. Droplet size and velocity in dual continuous horizontal oil-water flows. Chemical Engineering Research and Design 86, 83-93. http://dx.doi.org/10.1016/j.cherd.2007.10.012

Angeli, P., Hewitt, G.F., 1999. Pressure gradient in horizontal liquid-liquid flows. Int J Multiphas Flow 24, 1183-1203. http://dx.doi.org/10.1016/S0301-9322(98)00006-8

Angeli, P., Hewitt, G.F., 2000. Drop size distributions in horizontal oil-water dispersed flows. Chemical Engineering Science 55, 3133-3143.

Brauner, N., 2001. The prediction of dispersed flows boundaries in liquid-liquid and gas-liquid systems. Int J Multiphas Flow 27, 885-910. DOI: 10.1016/S0301-9322(00)00056-2

Brown, D.E., Pitt, L., 1972. Drop size distribution of stirred non-coalescing liquid-liquid system. Chemical Engineering Science 27, 577-583.

Cabellos, E.M., Carvalho, M.S., Ponce, R.V., 2009. Oil-in-water emulsion formation in laminar flow through capillaries. 20th International Congress of Mechanical Engineering, Gramado.

Calabrese, R.V., Chang, T.P.K., Dang, P.T., 1986. Drop Breakup in Turbulent Stirred-Tank Contactors, Part1: Effect of Dispersed-Phase Viscosity. AIChE Journal 32, 657-666.

Coulaloglou, C.A., Tavlarides, L.L., 1976. Drop Size Distribution and Coalescence Frequencies of Liquid-Liquid Dispersions in Flow Vessels. AIChE Journal 22, 289-297.

El-Hamouz, A.M., Stewart, A.C., 6-9 October 1996. On-line measurement of oil-water dispersion using a Par-Tec M300 laser backscatter instrument. SPE Annual Technical Conference, Denver.

Giapos, A., Pachatouridis, C., Stamatoudis, M., 2005. Effect of the number of impeller blades on the drop sizes in agitated dispersions. Chemical Engineering Research and Design 83, 1425-1430.

Hesketh, R.P., Russel, T.W.F., Etchells, A.W., 1987. Bubble size in horizontal pipelines. AIChE Journal 33, 663-667.

Hinze, J., 1955. Fundamentals of the hydrodynamic mechanism of splitting in dispersion processes. AIChE Journal 1, 289-295.

Ioannou, K., 2006. Phase Inversion Phenomenon in Horizontal Dispersed Oil/Water Pipeline Flows. PhD Thesis. University College London,

Kubie, J., Gardner, G.C., 1977. Drop sizes and drop dispersion in straight horizontal tubes and in helical coils. Chemical Engineering Science 32, 195-202. http://dx.doi.org/10.1016/0009-2509(77)80105-X

Lim, J.S., Wong, S.F., Law, M.C., Samyudia, Y., Dol, S.S., 2015. A review on the effects of emulsions on flow behaviours and common factors affecting the stability of emulsions. Journal of Applied Sciences 15, 167-172. 10.3923/jas.2015.167.172

Lovick, J., Angeli, P., 2004. Droplet size and velocity profiles in liquid-liquid horizontal flows. Chemical Engineering Science 59, 3105-3115. DOI:10.1016/j.ces.2004.04.035

Middleman, S., 1974. Drop Size Distributions Produced by Turbulent Pipe Flow of Immiscible Fluids through a Static Mixer. Ind. Eng. Chem. Process Des. Dev. 13, 78-83. DOI: 10.1021/i260049a015

Morales, R., Pereyra, E., Wang, S., Shoham, O., 2013. Droplet formation through centrifugal pumps for oil-in-water dispersions. SPE Journal 18, 172-178. http://dx.doi.org/10.2118/163055-PA

Noïk, C., Dalmazzone, C., Galinat, S., Masbernat, O., Guiraud, P., 2005. Flow of concentrated oil-water dispersion through a restriction. 12th International Conference on Multiphase Production Technology, Barcelona.

Pal, R., 1993. Pipeline Flow of Unstable and Surfactant-Stabilized Emulsions. AIChE Journal 39, 1754-1764. DOI: 10.1002/aic.690391103

Pal, R., 1996. Effect of Droplet Size on Rheology of Emulsions. AIChE Journal 42, 3181-3190. DOI: 10.1002/aic.690421119

Schümann, H., Khatibi, M., Tutkun, M., Pettersen, B.H., Yang, Z., Nydal, O.J., 2015. Droplet Size Measurements in Oil-Water Dispersions: A Comparison Study Using FBRM and PVM. Journal of Dispersion Science and Technology 36, 1432-1443. http://dx.doi.org/10.1080/01932691.2014.989569

Schümann, H., Tutkun, M., Yang, Z., Nydal, O.J., Experimental study of dispersed oil-water flow in a horizontal pipe with enhanced inlet mixing, Part 1: Flow paterns, phase distributions and pressure gradients. Submitted to the Journal of Petroleum Science and Engineering.

Simmons, M.J.H., Azzopardi, B.J., 2001. Drop size distributions in dispersed liquid-liquid pipe flow. Int J Multiphas Flow 27, 843-859. Doi 10.1016/S0301-9322(00)00055-0

Sleicher Jr., C.A., 1962. Maximum Stable Drop Size in Turbulent Flow. AIChE Journal 8, 471-477. DOI: 10.1002/aic.690080410

Sprow, F.B., 1967. Distribution of drop sizes produced in turbulent liquid-liquid dispersion. Chemical Engineering Science 22, 435-442.

van der Zande, M.J., van den Broek, W.M.G.T., 1998. Break-up of oil droplets in the production system. Proceedings of ASME Energy Sources Technology Conference and Exhibition, Housten.

Ward, J.P., Knudsen, J.G., 1967. Turbulent Flow of Unstable Liquid-Liquid Dispersions: Drop Sizes and Velocity Distributions. AIChE Journal 13, 356-365. DOI: 10.1002/aic.690130229

Zhou, G., Kresta, S.M., 1998. Correlation of mean drop size and minimum drop size with the turbulence energy dissipation and the flow in an agiated tank. Chemical Engineering Science 53, 2063-2079.